Carbohydrate Polymers 91 (2013) 377–384

Contents lists available at SciVerse ScienceDirect

Carbohydrate Polymers

journal homepage: www.elsevier.com/locate/carbpol

Morphology and thermal properties of PLA–cellulose nanofibers composites

Adriana N. Frone[a], Sophie Berlioz[b], Jean-François Chailan[b], Denis M. Panaitescu[a,*]

[a] Polymer Department, National Institute of Research and Development in Chemistry and Petrochemistry ICECHIM, 202 Splaiul Independentei, 060021 Bucharest, Romania
[b] Laboratoire Matériaux Polymères-Interfaces-Environnement Marin (MAPIEM), Institut Des Sciences De L'Ingenieur De Toulon Et Du Var, Université du Sud Toulon Var, Avenue Georges Pompidou, BP 56-83162 La Valette du Var Cedex, France

ARTICLE INFO

Article history:
Received 12 June 2012
Received in revised form 27 July 2012
Accepted 17 August 2012
Available online 24 August 2012

Keywords:
Cellulose nanofibers
Polylactic acid (PLA)
Biodegradable nanocomposites
AFM
Thermal properties

ABSTRACT

Biodegradable nanocomposites were obtained from polylactic acid (PLA) and cellulose nanofibers with diameters ranging from 11 nm to 44 nm. The influence of treated (with 3-aminopropyltriethoxysilane) and untreated nanofibers on the thermal properties of PLA was investigated in detail using multiple session Differential Scanning Calorimetry (DSC) analysis. The nucleating effect of the cellulose nanofibers was confirmed by all the DSC runs (two melting and two crystallization steps). The morphology of both neat PLA and nanocomposites was explored for the first time using a new powerful AFM technique, Peak Force QNM (Quantitative Mechanical Property Mapping at the Nanoscale), which emphasized the nanolevel characteristics by elastic modulus mapping. QNM analyses showed a better dispersion of the silane treated nanofibers in the matrix as compared to the untreated ones. Moreover, a higher degree of crystallinity was detected in the PLA composites containing untreated nanofibers compared to the composites with treated ones.

1. Introduction

The research interest of the polymer community on the production and the study of different biodegradable polymers that could replace petroleum-based plastics in all kinds of applications are constantly growing. Polylactic acid is one of the most studied biodegradable polymers mainly because of its high mechanical properties and the easy production from its monomer (i.e. lactic acid). At present, the majority of lactic acid used for the PLA production is produced by fermentation from agricultural products (e.g. corn, potato, cane sugar, and rice). The high biocompatibility and biodegradability of PLA make it a very good candidate for biomedical and packaging applications. Moreover, PLA can be readily processed similar to polyolefins. In spite of all these advantages, its range of application is still limited by its high production cost, its brittleness and its low thermal stability. The addition of renewable and biodegradable fillers like cellulose or cellulose derivatives could optimize the cost-performance balance and improve the mechanical and thermal behaviors (Oksman, Skrifvars, & Selin, 2003). The use of natural fibers in polymer composites to replace synthetic fibers like glass, receives an increasing attention because of their advantages such as abundance, renewability, high stiffness, non-abrasiveness to the processing equipment, possibility to be incinerated, low density and low cost. Hence, cellulose nanofibers have been tested to reinforce different polymeric matrices like starch (Chen, Liu, Chang, Cao, & Anderson, 2009; Kaushik, Singh, & Verma, 2010; Wu, Wang, Li, Li, & Wang, 2009), polyvinyl alcohol (Ibrahim, El-Zawawy, & Nassar, 2010; Lee et al., 2009), polylactic acid (Dobreva et al., 2010; Fortunati et al., 2012; Jonoobi, Harun, Mathew, & Oksman, 2010; Nakagaito, Fujimura, Sakai, Hama, & Yano, 2009; Pandey, Lee, & Ahn, 2010; Sanchez-Garcia & Lagaron, 2010; Si, Massa, Dalnoki Veress, Brown, & Jones, 2012) and other polymers (Awal, Ghosh, & Sain, 2010; Cherian et al., 2011; Xu, Kawata, Hosoi, Kawai, & Kuroda, 2009). A study dealing with the effect of microfibrillated cellulose (MFC) on the thermal and mechanical properties of PLA, demonstrated by DSC and DMA analyses that the use of MFC as fillers could extend PLA application range for products exposed to high temperature (Suryanegara, Nakagaito, & Yano, 2009). Moreover, it was shown that the addition of 20 wt.% of MFC increased the storage modulus of neat PLA from 293 MPa to 1034 MPa, respectively.

To extent their industrial applications, cellulose nanofibers must overcome their weak compatibility with hydrophobic polymer matrices in order to enhance the dispersion and to increase the stress transfer towards the matrix. To reduce the hydrophilic character of cellulose nanofibers and so, improve the adhesion properties, one of the most used methods is to chemically modify their surface. In this optic, several types of reagents have been studied among which anhydrides, isocyanates and organosilanes are the most representative (Lu, Askeland, & Drzal, 2008; Stenstad, Andresen, Tanem, & Stenius, 2008). In cellulose nanofibers

* Corresponding author. Tel.: +40 21 316 30 68; fax: +40 21 312 34 93.
E-mail address: panaitescu@icf.ro (D.M. Panaitescu).

0144-8617/$ – see front matter © 2012 Elsevier Ltd. All rights reserved.
http://dx.doi.org/10.1016/j.carbpol.2012.08.054

composites, silane reagents constitute the main used agents for different reasons: the modification of the surface properties of the nanofibers, the improvement of the mechanical performance due to an increase of the adhesion between fibers and matrix and the reduction of the water uptake of the composites. The efficiency of the silane treatment depends on many factors including organofunctionality of the silane, reaction time, temperature and pH. For example, Gregorova, Hrabalova, Wimmer, Saake, and Altaner (2009) reported an improvement of the thermal and mechanical properties of PLA reinforced with Stika fibers treated with vinyltrimethoxysilane. Unsaturated polyester and epoxy resins were reinforced with cellulose fibers treated with four different coupling agents: γ-aminopropyltriethoxysilane (APS), γ-methacrylopropyltrimethoxysilane (MPS), hexadecytrimethoxysilane (HDS) and mercaptopropylsilane (MRPS) (Abdelmouleh, Boufi, Belgacem, Dufresne, & Gandini, 2005). An increase of the modulus and tensile strengths in the resulted composites was observed. The influence of cellulose nanofibers in PLA was intensively studied by DSC. Some authors emphasized an increase of both the crystallinity and the melting point of the PLA when small amounts of cellulose nanofibers (1–5 wt.%) were used (Sanchez-Garcia & Lagaron, 2010). Others have found no significant influence of cellulose nanofibers when they were added in small quantity (Petersson & Oksman, 2006). Atomic force microscopy (AFM) was efficiently used to investigate polymer composites containing different types of cellulose fillers (Pakzad, Simonsen, & Yassar, 2012; Morsi, Pakzad, Amin, Yassar, & Heiden, 2011; Qu, Gao, Wu, & Zhang, 2010) emphasizing important features of these materials like the dispersion of the filler or polymer–cellulose filler interface characteristics. At this moment, AFM by QNM mode is the most suitable tool to determine the nanomechanical properties of material surface due to its ability to measure forces up to piconewton range. By our knowledge, morphological changes of PLA containing cellulose nanofibers were not investigated by AFM using Peak Force QNM.

In this work, cellulose nanofibers isolated by acid treatment of commercial microcrystalline cellulose were used to prepare composites with polylactic acid by melt compounding. The aim of the present investigation was to study the influence of the untreated and silane treated cellulose nanofibers on the thermal and morphological characteristics of PLA. For this purpose, the thermal properties of PLA and nanocomposites were investigated in detail using multiple session DSC analysis (heat–cool–heat–cool). The morphology of both PLA and nanocomposites was explored for the first time using a new powerful AFM technique, Peak Force QNM, which emphasized the nanolevel characteristics by elastic modulus mapping.

2. Experimental

2.1. Materials

A polylactic acid (PLA), trade name 4032D, from Nature Works® with a density of 1.24 g/cm^3 and a melting point of 160 °C was used as matrix. The tensile modulus and elongation at break were 3784 MPa (D882) and 100% (D822), respectively, as reported by the manufacturer. Microcrystalline cellulose (MCC) purchased from Sigma–Aldrich, was used for the production of cellulose nanofibers. MCC has a mean particle size of 20 μm as determined by SEM analysis (image not shown here) and was previously reported by Panaitescu et al. (2007). Sulfuric acid (H_2SO_4) 96% for the cellulose nanofibers isolation was obtained from Chimopar, Romania. 3-Aminopropyltriethoxysilane (APS) supplied by Sigma–Aldrich was used without any purification for the surface modification of the nanofibers.

2.2. Isolation of cellulose nanofibers

Cellulose nanofibers were isolated from MCC by applying the acid hydrolysis methodology described by Bondeson, Mathew, and Oksman (2006) but using different conditions. Briefly, MCC particles were dispersed in distillated water (1/10 wt.%) and the resulted suspension was placed in an ice bath and stirred. The concentrated sulfuric acid was added drop by drop until the desired acid concentration of 63% was reached. The suspension was then stirred vigorously for 10 h at 40 °C. After the hydrolysis process, the suspension containing cellulose nanofibers (CNF) showed a milky colloidal appearance. The obtained mixture was centrifuged and washed with distillated water using repeated cycles (20 min at 7000 rpm, Universal 320R Ultracentrifuge) until a pH of 4 was reached and ultrasonicated (Elmasonic S40H, Elma) for 5 h in an ice bath.

2.3. Surface modification of cellulose fibers

A 90/10 ethanol/water mixture containing 10% of APS was added to the water suspension of CNF. The final suspension was then stirred for 2 h at room temperature and then heated under reflux for 3 h resulting treated cellulose nanofibers (CNFS).

2.4. PLA cellulose nanofibers composites preparation

Both PLA pellets and cellulose nanofibers (CNF and CNFS) were dried in a vacuum oven for 9 h at 80 °C and 24 h at 30 °C, respectively. Immediately after drying, PLA was melt blended with cellulose nanofibers using a fully automated laboratory two roll mill from Brabender (Polymix 110L). Compounding was carried out at temperature of 165 ± 3 °C for 10 min and a rotor speed of 27/22.5 min^{-1}. Two blends containing 2.5 wt.% of silanized and unsilanized cellulose nanofibers, respectively were investigated in this work. Unfilled PLA was also melt-processes in the same conditions in order to prepare a reference material. To study the real effect of the nanofibers on the PLA, it is essential to compare samples which underwent exactly the same thermal history, including the blending step, otherwise some behavior differences may be erroneously attributed to the fillers. Then, 0.5 mm thick sheets were prepared from each composite by compression molding using an electric heated press. The compression molding was carried out at 180 °C, with a pre-heating stage at 50 atm for 3 min and a pressing stage at 150 atm for 2 min. The cooling of the resulted composite sheets was performed under pressure. A neat PLA sheet was prepared under the same conditions and served as a reference.

2.5. Methods

2.5.1. Atomic force microscopy (AFM) analysis of cellulose nanofibers

The structural properties of both cellulose nanofibers and PLA/cellulose nanofibers composites were studied using an atomic force microscope (AFM) from Bruker, Santa Barbara, equipped with a Nanoscope V controller and a MultiMode head. The aqueous suspensions of cellulose nanofibers were diluted, and one drop was dried on a glass substrate plate under vacuum for several hours. The equipment was operated in tapping mode using etched silicon tip (nominal radius 8 nm) with a cantilever length of 225 μm and a resonance frequency of about 75 kHz. AFM measurements were performed at room temperature with a scan rate of 1 Hz and a scan angle of 0°. The height and the amplitude of the signal were recorded simultaneously.

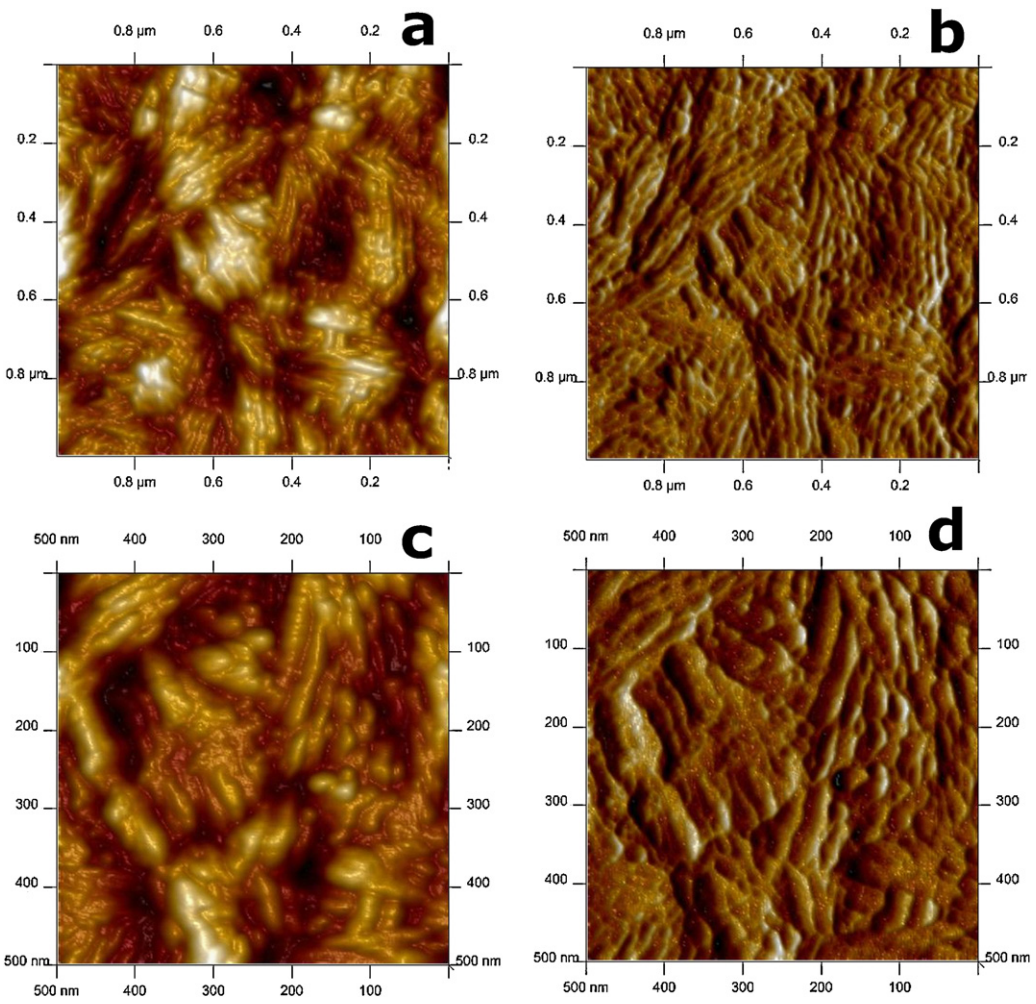

Fig. 1. Tapping mode AFM height (left) and amplitude images (right) of cellulose nanofibers type CNF: 1 μm × 1 μm (a) and (b); 500 nm × 500 nm (c) and (d).

2.5.2. Atomic force microscopy (AFM) analysis of PLA and nanocomposites

The dispersion of cellulose nanofibers in the PLA matrix was investigated by ScanAsyst AFM technique. The images (256 × 256) were recorded using scanning rates of 1.4 Hz and a scan angle of 90°. The nominal spring constant and nominal resonant frequency was 0.4 N/m and 70 kHz, respectively. Composite films with a uniform surface and a thickness of ~30 μm were used for AFM investigations. They were obtained from compression molded plates using a laboratory press type P200 E (Dr. Collin) under the following conditions: a pressing step of 3 min at 170 °C under 150 atm and a rapid cooling to avoid PLA crystallization.

AFM Peak Force QNM was used to investigate nanolevel mechanical properties of neat PLA and nanocomposites. Detailed description of Peak Force QNM mode is shown elsewhere (Morsi et al., 2011). AFM images of neat PLA and PLA composite films were captured in air under ambient condition with scanning rates ≤1 Hz and a scan angle of 90°. A silicon tip (nominal radius 8 nm) with a spring constant of 3 N/m and a resonant frequency of 75 kHz was used for the images recording (256 × 256). The elastic modulus was calculated by NanoScope software using the Derjaguin–Muller–Toropov (DMT) model (Derjaguin, Muller, & Toropov, 1975). The films used in QNM analysis were obtained in the same conditions mentioned above, with the difference of a slow cooling process. All AFM data analysis and image processing were made with NanoScope software version 1.20.

2.5.3. Differential Scanning Calorimeter (DSC) analysis

The melting and crystallization behaviors of PLA/cellulose nanofibers composites were studied using a Differential Scanning Calorimeter (DSC Q 100, TA Instruments) equipped with a refrigerated cooling system (RCS90). The samples of ~10 mg were heated from 40 to 200 °C and cooled back to 40 °C at a rate of 2 °C/min under a 50 mL/min nitrogen flow. This heating/cooling cycle is repeated one time at the same rate. Samples were sealed into aluminum pans and, an empty aluminum pan with the same weight as the sample pan was used as reference. Based on the endothermic and exothermic peaks all the characteristic temperatures and associated enthalpies were calculated with the same integration limits. The degree of crystallinity (X_c) of the PLA and its composites was calculated from the first thermal scan as follows:

$$X_c = \frac{\Delta H_m}{w \times \Delta H_{mo}} \times 100 \quad (1)$$

where ΔH_m and ΔH_{mo} are the melting enthalpies for PLA composites and the 100% crystalline PLA, respectively; w is the mass fraction of PLA in the composite. The melting enthalpy of a totally crystalline PLA material (ΔH_{mo}) was considered to be 93 J/g (Liu, Dever, Fair, & Benson, 1997). An overall accuracy of ±0.5 °C in temperature and ±1% in enthalpy was estimated.

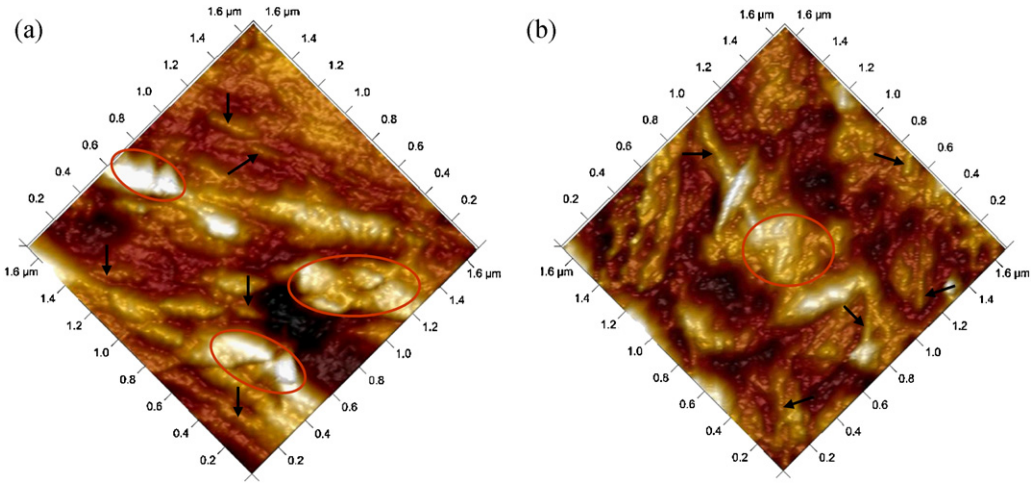

Fig. 2. AFM ScanAsyst – images of untreated (a) and treated (b) CNF reinforced PLA composites at a scan size of 1.7 μm × 1.7 μm. (For interpretation of the references to color in the text, the reader is referred to the web version of the article.)

3. Results and discussion

3.1. AFM investigation of cellulose nanofibers

Typical tapping mode AFM images of nanofibers obtained after acid hydrolysis and deposited on a glass substrate are shown in Fig. 1a–d. AFM height and amplitude images showed bundles of cellulose nanofibers with ribbon like shape structure. From these pictures, it is obvious that a considerable reduction in fiber size has been accomplished by the acid treatment considering an average size of 20 μm for the raw MCC cellulose. The diameter of individual fibers ranges from 11 to 44 nm with an average of 20 ± 6 nm. In order to have a representative value, this diameter was calculated on 70 fibers measurements with NanoScope software. To ensure the repeatability and the accuracy of the AFM scanning, different zones of the same sample were analyzed and the presented images are representative of the totality of the sample.

3.2. Morphology of neat PLA and PLA composites determined by AFM

3.2.1. Cellulose nanofibers dispersion in PLA composites by ScanAsyst AFM

Fig. 2a and b shows typical topographic images of PLA composites containing silane treated and untreated cellulose nanofibers. The comparative observation of these figures shows a better dispersion in the case of PLA composite containing CNFS. Several areas with CNF agglomerations marked with red circles (light grey in printed version) and individual nanofibers covered by the polymer (marked with black arrows) can be observed in Fig. 2a. A distinct improvement of the dispersion quality is observed when the nanofibers are silane treated (Fig. 2b). CNFS are more uniformly distributed on the surface of PLA/CNFS composite and less agglomerated fibers can be seen in Fig. 2b as compared to Fig. 2a. Most of CNF agglomerates are located at the surface of the material as opposite to CNFS which are located deeper in the polymer, suggesting a better cellulose fiber–matrix interface in the second case. Moreover, a different maximum height must be noted in the analyzed images: 27.3 nm for PLA/CNF and only 16.2 nm for PLA/CNFS confirming the deeper location in the matrix and the better adhesion. This improvement of the dispersion and adhesion is consistent with our previous SEM characterizations (Frone, Berlioz, Chailan, Panaitescu, & Donescu, 2011).

3.2.2. Influence of cellulose nanofibers on nanomechanical properties of PLA matrix

Peak Force QNM-modulus image (scanning area 3 μm × 3 μm) of neat PLA matrix, without any thermal treatment, is shown in Fig. 3a. From this image, the presence of crystallites is clearly evidenced in PLA. The matrix presents an organized structure composed of high modulus (light-colored) areas alternating with low modulus (dark-colored) areas. High modulus areas can be ascribed to the growing crystallites consisting of inclined stacks of lamellae. Henton, Gruber, Lunt, and Randall (2005) have shown that the crystallization of PLA at temperatures greater than 150 °C results in hexagonal lamellar stacking crystal morphology. Similar morphological trends were observed in Fig. 3a. At this stage, the crystallization process is not completed. An increase of the crystallization yield could be obtained after annealing. From our knowledge, AFM images illustrating the beginning of the crystallization process in PLA have not been previously presented.

Peak Force QNM images of PLA composites are presented in Fig. 3b and c. Many bright colored areas ascribed to cellulose fibers located close to the sample surface can be seen in the QNM – modulus images of the PLA composites (Fig. 3b and c). The cellulose fibers can be detected by QNM technique due to their significantly higher modulus than that of PLA matrix. Because of the inhomogeneous distribution of agglomerates in the case of PLA/CNF, some regions of the PLA are totally free from nanofibers, as can be seen in the middle of Fig. 3b. In these regions, a more organized structure is observed similar to the structure of the neat PLA. In PLA composite containing silane treated nanofibers (Fig. 3c) the lamellar crystalline structure is less obvious as in the previous case suggesting a lower crystallinity of PLA matrix. This observation will be confirmed by the DSC results.

3.3. Thermal behavior of PLA containing cellulose nanofibers

3.3.1. First heating–cooling run

DSC thermograms of the neat PLA and its nanocomposites, obtained from the first heating and cooling run at 2 °C/min, are shown in Fig. 4a. The PLA glass transition (T_g), followed by the polymer cold crystallization (T_{cc}) and the polymer melting can be observed on the thermograms of all samples. These three thermal events are typical for semi-crystalline PLA (Suryanegara, Nakagaito, & Yano, 2010). The DSC data and the degree of crystallinity (X_c) are reported in Table 1.

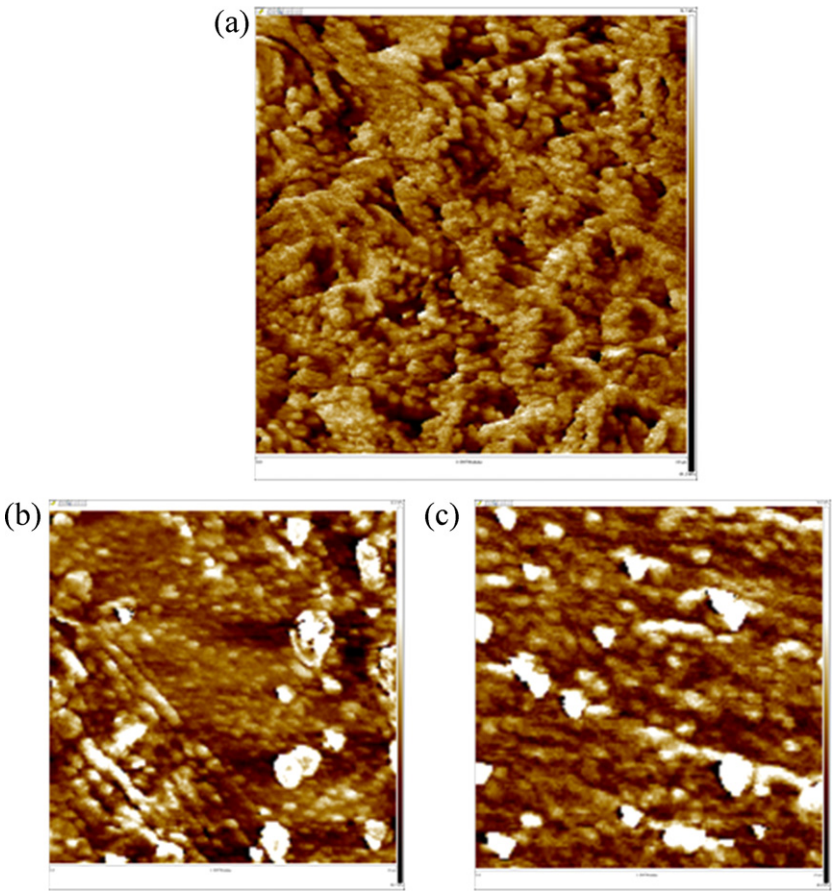

Fig. 3. AFM QNM – modulus images of neat PLA (a) and PLA composites reinforced with untreated (b) and treated cellulose nanofibers (c) at a scan size of 3 μm × 3 μm.

No significant modification of the glass transition temperature of the PLA is observed for this low weight fraction of cellulose fibers. It is known that the glass transition (T_g) is a complex phenomenon which depends on several factors including intermolecular interactions, steric effects, the chain flexibility, the molecular weight, the branching and the cross-linking density (Krishnamachari, Zhang, Lou, Yan, & Uitenham, 2009). Due to the low content of nanofillers, only a small fraction of PLA chains could see their mobility modified by the presence of nanofillers. The measure of T_g by DSC is not enough sensitive to detect this modification which implies only the small fraction of amorphous chains of PLA closed to the fillers. The shape of the DSC curves, with a slight endotherm overshoot in the glass transition could indicate a physical aging phenomenon, as already reported for PLA (Hernández-Sánchez et al., 2005). This phenomenon is particularly noticeable for the composites samples compared to the neat PLA.

Neat PLA and PLA nanocomposites exhibited two exothermic peaks, one above 85 °C and one just before the melting point of PLA, as shown in Fig. 4a. Due to the low cold crystallization temperature (Table 1), the PLA crystallization is not complete and an additional exothermic peak of crystallization appears. This peak is attributed to a melting/recrystallization mechanism which could be explained by an increase of the thickness of the crystalline lamellae formed during cold crystallization.

With the addition of cellulose nanofibers, the cold crystallization peak becomes broader and is shifted to lower temperatures as compared to the cold crystallization of neat PLA. The lower T_{cc} observed in the heating run can be an indication of faster crystallization induced by cellulose nanofillers which act as nucleating agents for PLA (Kang, Lee, Lee, Narayan, & Shin, 2008). Cellulose nanofibers allow heterogeneous nucleation mechanism which induces a decrease of the free energy barrier and fastens the crystallization. This observation is in agreement with the results of Suksut and Deeprasertkul (2011) related to the effect of nucleating agents on the thermal properties of PLA and PLA/natural rubber composites. The silane treatment of nanofibers induces a huge modification of the cold crystallization peak (Fig. 4a). In the case of PLA/CNFS, the peak is sharper and shifts to higher values than that of the neat PLA.

Table 1
DSC data corresponding to the first heating–cooling scan.

Sample	T_g (°C)	T_{cc} (°C)	ΔH_{cc}[a] (J/g)	T_c[b] (°C)	ΔH_c[c] (J/g)	T_m (°C)	ΔH_m (J/g)	T_{mc}[d] (°C)	ΔH_{mc}[e] (J/g)	X_c (%)
PLA	56.9	87.3	23.6	151.5	5.3	168.1	36.2	104.3	33.4	38.9
PLA/CNF	56.3	85.2	25.1	151.5	4.6	168.0	42.7	102.9	35.4	47.1
PLA/CNFS	57.2	89.8	25.4	151.4	5.0	167.9	37.3	101.1	30.5	41.1

[a] ΔH_{cc} – cold crystallization enthalpy.
[b] T_c – crystallization temperature.
[c] ΔH_c – crystallization enthalpy from the heating step.
[d] T_{mc} – melt crystallization temperature.
[e] ΔH_{mc} – melt crystallization enthalpy.

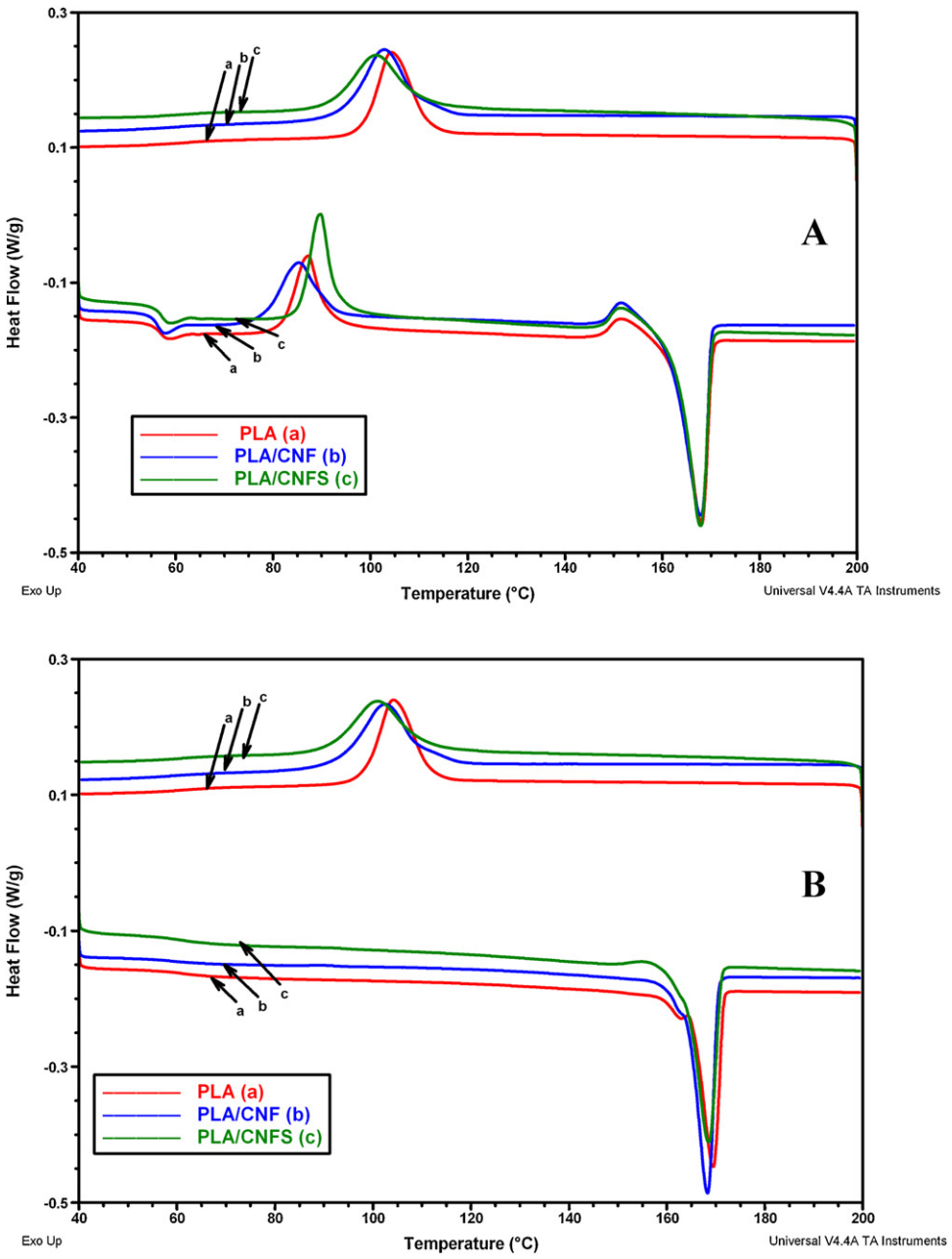

Fig. 4. DSC thermograms of neat PLA and PLA/cellulose nanofibers composites from the first (a) and second (b) heating–cooling runs.

In our opinion, this behavior is a result of the silane treatment which improves the adhesion to the matrix. The decrease of the mobility of the PLA chains which are close to the nanofibers could hinder the crystallization process and so lead to higher values of T_{cc}.

The endothermic peak corresponding to the fusion of the PLA crystallites (T_m) can be identified at around 168 °C for all the samples. By considering that the melting temperature depends on the size and the perfection of the crystalline lamellae (Liu & Donovan, 1995), we could suppose that the crystalline structure of the different materials obtained after the melting/recrystallization process are almost the same. The degree of crystallinity, calculated using Eq. (1), is higher for PLA nanocomposites than for neat PLA (Table 1). This increase of crystallinity confirms the previous observations related to the role of cellulose nanofibers as nucleating agents. Similar observations were made by other authors (Tokoro et al., 2008). By comparison between the two types of composites, a slight higher crystallinity yield is observed for the PLA/CNF composites as compared to the PLA/CNFS. The stronger adhesion between the PLA matrix and the CNFS due to the silane treatment could hinder the motion of the PLA chains which are close to the CNFS. This decrease of mobility could be an explanation of the lower crystalline ratio and the higher cold crystallization temperature. Our work also supports the concept of an increase of the polymer chains mobility when the polymer is confined near a non-interacting interface. It was postulated by Si, Massa, Dalnoki Veress, Brown, and Jones (2005) that an increase of the chain mobility near a non-interacting surface could be attributed to a reduction of the entanglement effect.

3.3.2. Second heating–cooling run

The DSC thermograms – obtained during the second heating scan for neat PLA and nanocomposites are shown in Fig. 4b. The

Table 2
DSC data corresponding to the second heating–cooling scan.

Sample	T_g (°C)	T_{m1} (°C)	ΔH_{m1}[a] (J/g)	T_{m2} (°C)	ΔH_{m2}[b] (J/g)	ΔH_m (J/g)	T_{mc} (°C)	ΔH_{mc} (J/g)
PLA	61.1	162.6	0.37	169.5	36.5	36.9	104.2	33.3
PLA/CNF	59.9	162.2	0.06	168.3	43.4	43.5	102.5	33.9
PLA/CNFS	60.3	162.6	0.02	168.6	38.1	38.1	101.0	29.4

[a] ΔH_{m1} – melt crystallization enthalpy from the first melting peak.
[b] ΔH_{m2} – melt crystallization enthalpy from the second melting peak.

thermograms of the composites present only the melting event. The glass transition temperature is hardly observed and the cold crystallization phenomenon is absent, indicating that the materials were highly crystalline after the previous cooling at 2 °C/min. It must be noted that a shoulder-melting peak appeared instead just before the main melting peak. The shoulder and the main transition were noticeable for all the samples and were noted T_{m1} and T_{m2}, respectively. Each melting peak is the signature of a crystalline lamellae population essentially characterized by its thickness or its perfection.

A comparison between the enthalpy of crystallization measured during the first cooling and the melting enthalpy obtained during the second heating scan indicated clear difference especially for composites. Hence, the enthalpies of melting were about 8 J/g higher than the enthalpies of crystallization in the case of nanocomposites indicating that, a crystallization phenomenon occurred during the second heating. A more careful observation of the thermograms of the nanocomposites reveals the presence of small endotherms just before the main melting peaks which could be one explanation for these differences of enthalpy. Otherwise, it was proved that the PLA crystals have a large tendency to reorganize into more stable structures through continuous partial melting–recrystallization–perfection mechanism during heating (Di Lorenzo, 2006). Consequently, the small or imperfect crystals created during previous cooling could reorganize and the reorganization of these crystals results in a multiple melting behavior. The melting peak at higher temperature (T_{m2}) could be attributed to a more perfect crystalline structure of PLA and the shoulder peak at lower temperature (T_{m1}) to a less perfect crystalline structure. Previous studies on PLA reported bimodal melting peak (He, Fan, Wei, & Li, 2006; Sim & Han, 2010; Suksut & Deeprasertkul, 2011). For example, Suksut and Deeprasertkul (2011) observed the presence of two populations of crystallites with different sizes and degrees of perfection. T_{m1} corresponding to defective crystals remains in the same range of temperature whatever the nanofibers were silanized or not. The total melting enthalpy (ΔH_m) of neat PLA and PLA/cellulose nanofibers composites, including both endothermic peaks, remained almost unchanged compared to the first temperature cycle (Table 2). Similar behavior relating to the degree of crystallinity and the variation of the characteristic temperatures (T_g and T_m) were observed in this second heating run.

4. Conclusions

In this study cellulose nanofibers prepared by acid hydrolysis, raw or silane treated, were used as reinforcement for PLA. Thermal properties of PLA and PLA modified with cellulose nanofibers were deeply investigated and the DSC results correlated well with morphological features observed by advanced AFM techniques.

Crystalline grains consisting of inclined stacks of PLA lamellae were observed by Peak Force QNM, emphasizing a beginning of PLA crystallization. QNM images showed an improved dispersion of cellulose nanofibers in PLA after silane treatment.

DSC measurements revealed higher degree of crystallinity for the composites containing untreated nanofibers and demonstrated the role of cellulose nanofibers as nucleating agents. Improved adhesion between the silanized nanofibers and PLA could explain the lower crystallinity content and the higher cold crystallization temperature than for composites containing untreated fillers.

References

Abdelmouleh, M., Boufi, S., Belgacem, M. N., Dufresne, A., & Gandini, A. (2005). Modification of cellulose fibers with functionalized silanes: Effect of the fiber treatment on the mechanical performances of cellulose–thermoset composites. *Journal of Applied Polymer Science*, *98*, 974–984.

Awal, A., Ghosh, S. B., & Sain, M. (2010). Thermal properties and spectral characterization of wood pulp reinforced bio-composite fibers. *Journal of Thermal Analysis and Calorimetry*, *99*, 695–701.

Bondeson, D., Mathew, A., & Oksman, K. (2006). Optimization of the isolation of nanocrystals from microcrystalline cellulose by acid hydrolysis. *Cellulose*, *13*, 171–180.

Chen, Y., Liu, C., Chang, P. R., Cao, X., & Anderson, D. P. (2009). Bionanocomposites based on pea starch and cellulose nanowhiskers hydrolyzed from pea hull fibre: Effect of hydrolysis time. *Carbohydrate Polymers*, *76*, 607–615.

Cherian, B. M., Leão, A. L., de Souza, S. F., Costa, L. M. M., de Olyveira, G. M., Kottaisamy, M., et al. (2011). Cellulose nanocomposites with nanofibres isolated from pineapple leaf fibers for medical applications. *Carbohydrate Polymers*, *86*(4), 1790–1798.

Derjaguin, B. V., Muller, V. M., & Toropov, Y. P. (1975). Effect of contact deformations on the adhesion of particles. *Journal of Colloid and Interface Science*, *53*, 314–326.

Di Lorenzo, M. L. (2006). Calorimetric analysis of the multiple melting behavior of poly(L-lactic acid). *Journal of Applied Polymer Science*, *100*, 3145–3151.

Dobreva, T., Benavente, R., Perena, J. M., Perez, E., Avella, M., Garcıa, M., et al. (2010). Effect of different thermal treatments on the mechanical performance of poly(L-lactic acid) based eco-composites. *Journal of Applied Polymer Science*, *116*, 1088–1098.

Fortunati, E., Armentano, I., Zhou, Q., Iannoni, A., Saino, E., Visai, L., et al. (2012). Multifunctional bionanocomposite films of poly(lactic acid), cellulose nanocrystals and silver nanoparticles. *Carbohydrate Polymers*, *87*(2), 1596–1605.

Frone, A. N., Berlioz, S., Chailan, J.-F., Panaitescu, D. M., & Donescu, D. (2011). Cellulose fiber-reinforced polylactic acid. *Polymer Composites*, *32*, 976–985.

Gregorova, A., Hrabalova, M., Wimmer, R., Saake, B., & Altaner, C. (2009). Poly(lactide acid) composites reinforced with fibers obtained from different tissue types of *Picea sitchensis*. *Journal of Applied Polymer Science*, *114*, 2616–2623.

He, Y., Fan, Z., Wei, J., & Li, S. (2006). Morphology and melt crystallization of poly(L-lactide) obtained by ring opening polymerization of L-lactide with zinc catalyst. *Polymer Engineering and Science*, *46*, 1583–1589.

Henton, D. E., Gruber, P., Lunt, J., & Randall, J. (2005). Polylactic acid technology. In A. K. Mohanty, M. Misra, & L. T. Drzal (Eds.), *Natural fibers, biopolymers and biocomposites* (pp. 527–578). CRC Press.

Hernández-Sánchez, F., Molina Mateo, J., Romero Colomer, F. J., Salmerón Sánchez, M., Gómez Ribelles, J. L., & Mano, J. F. (2005). Influence of low-temperature nucleation on the crystallization process of poly(L-lactide). *Biomacromolecules*, *6*, 3283–3290.

Ibrahim, M. M., El-Zawawy, W. K., & Nassar, M. A. (2010). Synthesis and characterization of polyvinyl alcohol/nanospherical cellulose particle films. *Carbohydrate Polymers*, *79*, 694–699.

Jonoobi, M., Harun, J., Mathew, A. P., & Oksman, K. (2010). Mechanical properties of cellulose nanofiber (CNF) reinforced polylactic acid (PLA) prepared by twin screw extrusion. *Composites Science and Technology*, *70*(12), 1742–1747.

Kang, K. S., Lee, S. I., Lee, T. J., Narayan, R., & Shin, B. Y. (2008). Effect of biobased and biodegradable nucleating agent on the isothermal crystallization of poly(lactic acid). *Korean Journal of Chemical Engineering*, *25*, 599–608.

Kaushik, A., Singh, M., & Verma, G. (2010). Green nanocomposites based on thermoplastic starch and steam exploded cellulose nanofibrils from wheat straw. *Carbohydrate Polymers*, *82*(2), 337–345.

Krishnamachari, P., Zhang, J., Lou, J., Yan, J., & Uitenham, L. (2009). Biodegradable poly(lactic acid)/clay nanocomposites by melt intercalation: A study of morphological, thermal, and mechanical properties. *International Journal of Polymer Analysis and Characterization*, *14*, 336–350.

Lee, S. Y., Mohan, D. J., Kang, I. A., Doh, G. H., Lee, S., & Han, S. O. (2009). Nanocellulose reinforced PVA composite films: Effects of acid treatment and filler loading. *Fibers and Polymers*, *10*, 77–82.

Liu, Y., & Donovan, J. A. (1995). Miscibility and crystallization of semicrystalline nylon 6 and amorphous nylon 6IcoT blends. *Polymer*, *36*, 4797–4803.

Liu, X., Dever, M., Fair, N., & Benson, R. S. (1997). Thermal and mechanical properties of poly(lactic acid) and poly(ethylene/butylene succinate) blends. *Journal of Environmental Polymer Degradation*, *5*, 225–235.

Lu, J., Askeland, P., & Drzal, L. T. (2008). Surface modification of microfibrillated cellulose for epoxy composite applications. *Polymer*, *49*, 1285–1296.

Morsi, S. M., Pakzad, A., Amin, A., Yassar, R. S., & Heiden, P. A. (2011). Chemical and nanomechanical analysis of rice husk modified by ATRP-grafted oligomer. *Journal of Colloid Interface Science*, *360*, 377–385.

Nakagaito, A. N., Fujimura, A., Sakai, T., Hama, Y., & Yano, H. (2009). Production of microfibrillated cellulose (MFC)-reinforced polylactic acid (PLA) nanocomposites from sheets obtained by a papermaking-like process. *Composites Science and Technology*, *69*, 1293–1297.

Oksman, K., Skrifvars, M., & Selin, J.-F. (2003). Natural fibres as reinforcement in polylactic acid (PLA) composites. *Composites Science and Technology*, *63*, 1317–1324.

Pakzad, A., Simonsen, J., & Yassar, R. (2012). Gradient of nanomechanical properties in the interphase of cellulose nanocrystal composites. *Composites Science and Technology*, *72*, 314–319.

Panaitescu, D. M., Donescu, D., Bercu, C., Vuluga, D. M., Iorga, M., & Ghiurea, M. (2007). Polymer composites with cellulose microfibrils. *Polymer Engineering and Science*, *47*, 1228–1234.

Pandey, J. K., Lee, C. S., & Ahn, S. H. (2010). Preparation and Properties of bionanoreinforced composites from biodegradable polymer matrix and cellulose whiskers. *Journal of Applied Polymer Science*, *115*, 2493–2501.

Petersson, L., & Oksman, K. (2006). Biopolymer based nanocomposites: Comparing layered silicates and microcrystalline cellulose as nanoreinforcement. *Composites Science and Technology*, *66*, 2187–2196.

Qu, P., Gao, Y., Wu, G., & Zhang, L. (2010). Nanocomposites of poly(lactic acid) reinforced with cellulose nanofibrils. *BioResources*, *5*, 1811–1823.

Sanchez-Garcia, M. D., & Lagaron, J. M. (2010). On the use of plant cellulose nanowhiskers to enhance the barrier properties of polylactic acid. *Cellulose*, *17*, 987–1004.

Shi, Q., Zhou, C., Yue, Y., Guo, W., Wu, Y., & Wu, Q. (2012). Mechanical properties and in vitro degradation of electrospun bio-nanocomposite mats from PLA and cellulose nanocrystals. *Carbohydrate Polymers*, *90*(1), 301–308.

Si, L., Massa, M. V., Dalnoki Veress, K., Brown, H. R., & Jones, R. A. L. (2005). Chain entanglement in thin freestanding polymer films. *Physical Review Letters*, *94*, 127801–127805.

Sim, K. J., & Han, S. O. (2010). Dynamic mechanical and thermal properties of red algae fiber reinforced poly(lactic acid) biocomposites. *Macromoleular Research*, *18*, 489–495.

Stenstad, P., Andresen, M., Tanem, B. S., & Stenius, P. (2008). Chemical surface modifications of microfibrillated cellulose. *Cellulose*, *15*, 35–45.

Suksut, B., & Deeprasertkul, C. (2011). Effect of nucleating agents on physical properties of poly(lactic acid) and its blend with natural rubber. *Journal of Polymers and the Environment*, *19*, 288–296.

Suryanegara, L., Nakagaito, A. N., & Yano, H. (2009). The effect of crystallization of PLA on the thermal and mechanical properties of microfibrillated cellulose-reinforced PLA composites. *Composites Science and Technology*, *69*, 1187–1192.

Suryanegara, L., Nakagaito, A. N., & Yano, H. (2010). Thermo-mechanical properties of microfibrillatedcellulose-reinforced partially crystallized PLA composites. *Cellulose*, *17*, 771–778.

Tokoro, R., Vu, D. M., Okubo, K., Tanaka, T., Fujii, T., & Fujiura, T. (2008). How to improve mechanical properties of polylactic acid with bamboo fibers. *Journal of Materials Science*, *43*, 775–787.

Wu, R. L., Wang, X. L., Li, F., Li, H. Z., & Wang, Y. Z. (2009). Green composite films prepared from cellulose, starch and lignin in room-temperature ionic liquid. *Bioresources Technology*, *100*, 2569–2574.

Xu, Y., Kawata, S., Hosoi, K., Kawai, T., & Kuroda, S. (2009). Thermomechanical properties of the silanized-kenaf/polystyrene composites. *Express Polymer Letters*, *3*, 657–664.